Electrically induced *n-i-p* junctions in multiple graphene layer structures

M. Ryzhii* and V. Ryzhii
Computational Nanoelectronics Laboratory, University of Aizu, Aizu-Wakamatsu 965-8580, Japan and CREST, Japan Science and Technology Agency, Tokyo 107-0075, Japan

T. Otsuji
Research Institute of Electrical Communication, Tohoku University, Sendai 980-8577, Japan and CREST, Japan Science and Technology Agency, Tokyo 107-0075, Japan

V. Mitin
Department of Electrical Engineering, University at Buffalo–State University of New York, Buffalo, New York 14260, USA

M. S. Shur
Department of Electrical, Computer, and Systems Engineering, Rensselaer Polytechnic Institute, Troy, New York 12180, USA
(Received 8 February 2010; revised manuscript received 6 June 2010; published 19 August 2010)

The Fermi energies of electrons and holes and their densities in different graphene layers (GLs) in the *n* and *p* regions of the electrically induced *n-i-p* junctions formed in multiple-GL structures are calculated both numerically and using a simplified analytical model. The reverse current associated with the injection of minority carriers through the *n* and *p* regions in the electrically induced *n-i-p* junctions under the reverse bias is calculated as well. It is shown that in the electrically induced *n-i-p* junctions with moderate numbers of GLs the reverse current can be substantially suppressed. Hence, multiple-GL structures with such *n-i-p* junctions can be used in different electron and optoelectronic devices.

DOI: 10.1103/PhysRevB.82.075419 PACS number(s): 73.50.Pz, 73.63.−b

I. INTRODUCTION

The possibility to form electrically induced *n-p* and *n-i-p* junctions[1–3] in gated graphene layers (GLs), as well as lateral arrays of graphene nanoribbons and graphene bilayer, opens up prospects novel electronic and optoelectronic devices.[4–8] In contrast to chemically doped *n* and *p* regions, electrically induced *n-p* and *n-i-p* junctions, allow for voltage control. Recent success in fabricating high-quality multiple GLs (Refs. 9–11) (see also the recent review article[12] and references therein) stimulates an interest in different prospective devices using multiple-GL structures. These structures constitute the stacks of disoriented GLs (with the non-Bernal stacking). Each GL exhibits linear dispersion relation for electrons and holes similar to that in a single GL. This is a well-established experimental fact (see, for instance, Refs. 11–14). Using the multiple-GL structures instead of single-GL structures can provide a significant improvement in device performance of terahertz tunneling transit-time oscillators (similar to that considered in Ref. 4), lasers with optical and electrical pumping, and high-performance interband photodetectors.[15–17] Gated multiple-GL structures can be also used in high-frequency field-effect transistors[18] and other devices (such as terahertz frequency multipliers and plasmonic devices). However the penetration of the electric field (transverse to the GL plane) beyond the topmost GL as well as its screening by electron or hole charges in GLs can substantially limit the gate control (the effect of the quantum capacitance[19]). In this paper, we study the influence of screening in gated multiple-GL structures on the formation and characteristics of *n* or *p* regions and *n-i-p* junctions in these structures. We calculate the electron and hole Fermi energies and densities in GLs in the *n* and *p* regions as functions of the GL index, gate voltage, and temperature. Using these data, we find the voltage and temperature dependences of the reverse current in the *n-i-p* junctions with different structural parameters. The multiple-GL structures are often obtained by thermal decomposition from 4H-SiC substrate (see, for instance, Refs. 9 and 10) on the C-terminated surface. The majority of the top GLs is practically neutral, whereas a buffer bottom GL (BGL) or a few BGLs in the very close vicinity of the interface with SiC is highly conducting (doped) as a result of the charge transfer from SiC.[9] For the device applications akin those considered in Refs. 15–17, such a highly conducting BGL plays a negative role. Due to this, we focus on the multiple-GL structures in which the BGL (or BGLs) and, hence, the effect of SiC substrate are eliminated. The multiple-GL structures without the BGL (BGLs) can be fabricated using chemical/mechanical reactions and transferred substrate techniques, which include chemically etching the substrate and the highly conducting GL (or GLs) and transferring the upper portion of the multiple-GL structure on a Si or equivalent substrate. The mechanical peeling of the upper portion of GL with the subsequent placement on a substrate is another option. Possible modifications of the effects under consideration in the multiple-GL structures with the highly conducting BGL are briefly discussed below. The structures with few non-Bernal stacked GLs are also fabricated on 3C-SiC(110) on Si(110) substrate.[20]

 ©2010 The American Physical Society

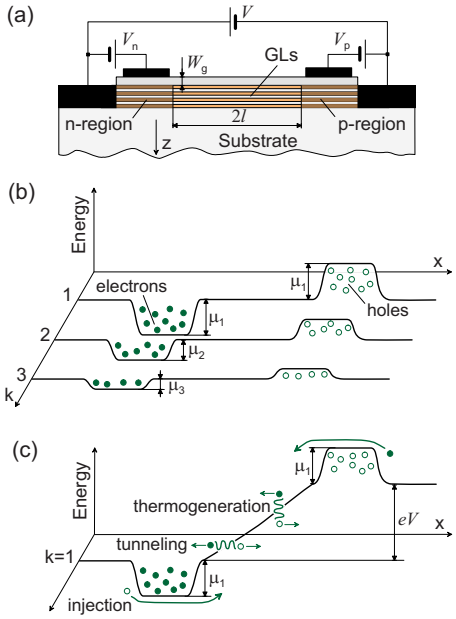

FIG. 1. (Color online) Schematic view of (a) a multiple-GL structure and its band diagrams at (b) zero bias voltage ($V=0$) and (c) at reverse bias (for GL with $k=1$). Arrows indicate the directions of propagation of injected electrons and holes as well as those thermogenerated and generated due to interband tunneling.

II. EQUATIONS OF THE MODEL

Let us consider a multiple-GL structure with the side Ohmic contacts to all GLs and two split gates (isolated from GLs) on the top of this structure as shown in Fig. 1(a). Applying the positive ($V_n=V_g>0$) or negative ($V_p=-V_g<0$) voltage between the gate and the adjacent contact (gate voltage), one can obtain the electrically induced n or p region. In the single- and multiple-GL structures with two split top gates under the voltages of different polarity, one can create lateral n-p or n-i-p junctions. Generally, the source-drain voltage V can be applied between the side Ohmic contacts to GLs. Depending on the polarity of this voltage, the n-p and n-i-p junctions can be either direct or reverse biased. We assume that the potentials of the first (source) contact and the pertinent gate are $\varphi_s=0$ and $\varphi_g=V_g>0$, respectively, and the potentials of another gate and contact (drain) are $\varphi_g=-V_g<0$ and $\varphi_d=V=0$ (or $\varphi_d=V\neq 0$. If the slot between the gates $2Lg$ is sufficiently wide (markedly exceeds the thickness of the gate layer W_g separating the gates and the topmost GL), there are intrinsic i regions in each GL under the slot. Thus the n-i-p junction is formed. The pertinent band diagrams are shown in Figs. 1(b) and 1(c). Since the side contacts are the Ohmic contacts, the electron Fermi energy in the kth GL sufficiently far from the contacts are given by $\mu_k=\pm e\varphi_k$. Here e is the electron charge and $\varphi_k=\varphi|_{z=kd}$ is the potential of the kth GL, $k=1,2,\ldots,K$, where K is the number of GLs in the structure, d is the spacing between GLs, and the axis z is directed perpendicular to the GL plane with $z=0$ corresponding to the topmost GL and $z=z_K=Kd$ to the lowest one.

Focusing on the n region (the p region can be considered in a similar way) and introducing the dimensionless potential $\psi=2\varphi/V_g$, one can arrive at the following one-dimensional Poisson equation governing the potential distribution in the z direction (in the n region):

$$\frac{d^2\psi}{dz^2}=\frac{8\pi e}{æ V_g}\sum_{k=1}^{K}(\Sigma_k^- - \Sigma_k^+)\cdot\delta(z-kd+d). \tag{1}$$

Here $æ$ is the dielectric constant, $\delta(z)$ and Σ_k^- and Σ_k^+ are the equilibrium sheet densities in the kth GL of electrons and holes, respectively. These densities, taking into account the linear dispersion low for electrons and holes in graphene, are expressed via the electron Fermi energy as

$$\Sigma_k^{\mp}=\frac{2}{\pi}\left(\frac{k_BT}{\hbar v_F}\right)^2\int_0^\infty\frac{d\xi\xi}{1+\exp(\xi\mp\mu_k/k_BT)}$$
$$=\frac{12\Sigma_T}{\pi^2}\int_0^\infty\frac{d\xi\xi}{1+\exp(\xi\mp\mu_k/k_BT)}, \tag{2}$$

where $\Sigma_T=(\pi/6)(k_BT/\hbar v_F)^2$ is the electron and hole density in the intrinsic graphene at the temperature T, $v_F\simeq 10^8$ cm/s is the characteristic velocity of electrons and holes in graphene, and $\hbar$ and k_B are the Planck and Boltzmann constants, respectively. Here it is assumed that the electron (hole) energy spectrum is $\varepsilon=v_Fp$, where p is the absolute value of the electron momentum. The boundary conditions are assumed to be as follows:

$$\psi|_{z=-0}=2+W_g\frac{d\psi}{dz}|_{z=-0},\quad \frac{d\psi}{dz}|_{z=z_K+0}=0. \tag{3}$$

Equations (1)–(3) yield

$$2-\psi_1=\Gamma\Phi(\psi_1) \tag{4}$$

for $K=1$

$$\frac{d}{W_g}(2-\psi_1)-\psi_1+\psi_2=\frac{d}{W_g}\Gamma\Phi(\psi_1),$$

$$\psi_1-\psi_2=\Gamma\Phi(\psi_2) \tag{5}$$

for $K=2$ and

$$\frac{d}{W_g}(2-\psi_1)-\psi_1+\psi_2=\frac{d}{W_g}\Gamma\Phi(\psi_1),$$

$$\psi_{k-1}-2\psi_k+\psi_{k+1}=\frac{d}{W_g}\Gamma\Phi(\psi_k),\quad (2\le k\le K-1),$$

$$\psi_{K-1}-\psi_K=\frac{d}{W_g}\Gamma\Phi(\psi_K) \tag{6}$$

for $K>2$. Here

$$\Phi(\psi)=\frac{12}{\pi^2}\left[\int_0^\infty\frac{d\xi\xi}{1+\exp(\xi-U_g\psi)}-\int_0^\infty\frac{d\xi\xi}{1+\exp(\xi+U_g\psi)}\right], \tag{7}$$

where $\Gamma=(8\pi/æ)(eW_g\Sigma_T/V_g)\propto T^2/V_g$ and $U_g=eV_g/2k_BT$.

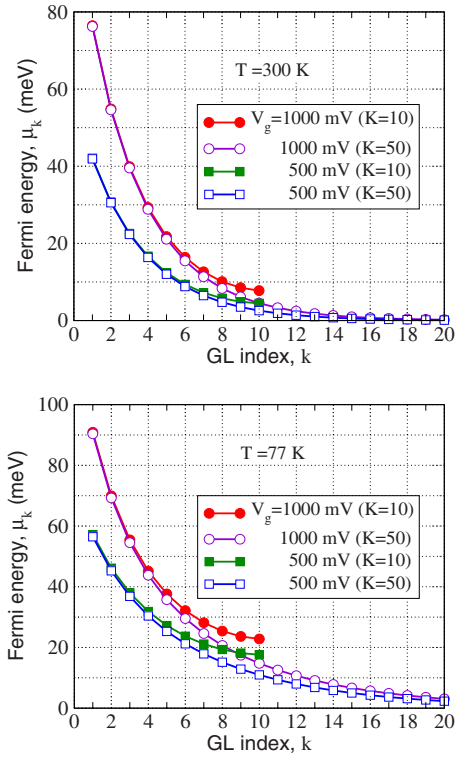

FIG. 2. (Color online) The electron Fermi energy μ_k as a function of the GL index k calculated for multiple-GL structures with different number of GLs K for different gate voltages V_g at $T=300$ K (upper panel) and $T=77$ K (lower panel).

III. NUMERICAL RESULTS

Equations (4)–(7) were solved numerically. The results of the calculations are shown in Figs. 2–5. In these calculations, we assumed that $\varkappa=4$, $d=0.35$ nm, and $W_g=10$ nm.

Figure 2 shows the dependences of the electron Fermi energy

$$\mu_k = \frac{eV_g}{2}\psi_k \tag{8}$$

as a function of the GL index k calculated for multiple-GL structures with different number of GLs K at different gate voltages and temperatures. One can see that the Fermi energy steeply decreases with increasing GL index. However, in GLs with not too large k, the Fermi energy is larger or about of the thermal energy. As one might expect, the electron Fermi energies in all GLs at $T=77$ K are somewhat larger than at $T=300$ K (see also Fig. 5). The obtained values of the electron Fermi energies in topmost GLs are $\mu_1 \simeq 92$ meV and $\mu_1 \simeq 77$ meV for $V_g=1000$ mV at $T=77$ K and $T=300$ K, respectively.

Figure 3 shows the voltage dependences of the electron Fermi energies in some GLs in multiple-GL structure with $K=2$, $K=10$, and $K=50$ at $T=300$ K. Figure 4 shows the electron densities Σ_k^- in the structures with different number of GLs K at different temperatures. One can see that the calculated electron densities in GLs with sufficiently large indices ($k>15$ at $T=77$ K and $T=300$ K) approach to their values in the intrinsic graphene ($\Sigma_T=0.59\times10^{10}$ cm^{-2} and 8.97×10^{10} cm^{-2}). The electron densities in GLs in the structures with different K are rather close to each other, particularly, in GLs with small and moderate indices.

Figure 5 presents the Fermi energies in GLs with different indices at different temperatures. One can see from Fig. 5 (as well as from Fig. 2) that the higher T corresponds to lower μ_k. This is due to an increasing dependence of the density of states on the energy and the thermal spread in the electron energies.

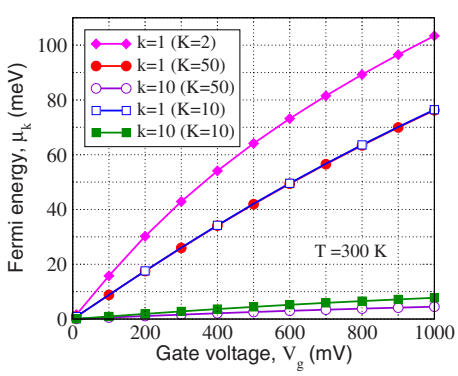

FIG. 3. (Color online) Voltage dependences of electron Fermi energies in some GLs in multiple-GL structure with different K at $T=300$ K.

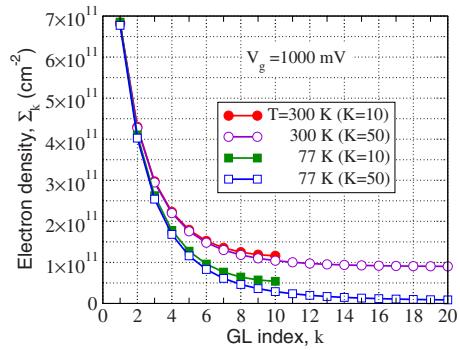

FIG. 4. (Color online) Electron density vs GL index in multiple-GL structures with different number of GLs ($K=10$ and $K=50$) at different temperatures and $V_g=1000$ mV.

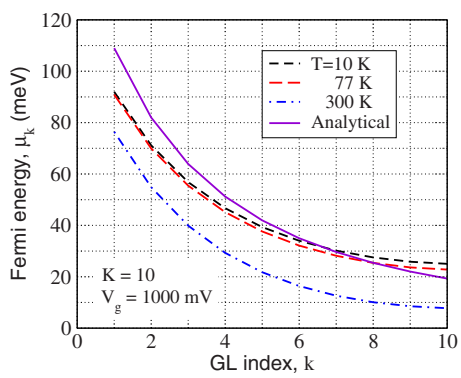

FIG. 5. (Color online) Comparison of the μ_k vs k dependences calculated for different temperatures using numerical and simplified analytical (solid line) models.

IV. ANALYTICAL MODEL

At not too low gate voltages when $U_g \gg 1$, one can assume that in a number of GLs the electrons under the gate are degenerate, i.e., $\mu_k \gg k_B T$, and the contribution of holes (nondegenerate) can be disregarded, hence, from Eq. (7) we obtain

$$\Phi(\psi) \simeq \frac{6}{\pi^2} U_g^2 \psi^2. \tag{9}$$

In this case, for a single-GL structure ($K=1$), Eq. (4) yields

$$2 - \psi_1 \simeq \frac{6}{\pi^2} \Gamma U_g^2 \psi_1^2. \tag{10}$$

Solving Eq. (10) and considering Eq. (8), for the electron Fermi energy in a GL (in a single-GL structure), we obtain

$$\mu_1 \simeq \mu_g \sqrt{1 - \frac{\mu_g}{eV_g}}, \tag{11}$$

where $\mu_g = \hbar v_F \sqrt{\varkappa V_g / 4eW_g}$. For the same parameters as those used in Figs. 2–4, $\mu_1 \simeq 150$ meV. Such a value is markedly larger than those calculated for the topmost GLs in multiple-GL structures (although it is somewhat exaggerated because the temperature spread in the electron energies is disregarded). This can be attributed to the fact that in multiple-GL structures the electron density is shared between the topmost GL and underlying GLs resulting in lower Fermi energies in all of them.

Considering multiple-GL structure with large K, one can neglect the discreteness of the structure and replace the summation in Eq. (1) by the integration. As a result, following Ref. 17, one can arrive at

$$\frac{d^2\psi}{dz^2} = 0 \quad (-W_g < z < 0, z > z_K), \tag{12}$$

$$\frac{d^2\psi}{dz^2} = \frac{\Gamma}{dW_g} \Phi(\psi) \quad (0 < z < z_K). \tag{13}$$

In this case, considering Eq. (7), we arrive at

$$\frac{d^2\psi}{dz^2} = \frac{\psi^2}{L_s^2} \tag{14}$$

with the characteristic screening length

$$L_s = \frac{\pi\sqrt{dW_g}}{\sqrt{6\Gamma} U_g} = \hbar v_F \sqrt{\frac{\varkappa d}{2e^3 V_g}} \propto V_g^{-1/2}. \tag{15}$$

The boundary conditions for Eq. (14) are given by Eq. (3)

In multiple-GL structures with a large number of GLs ($K \gg 1$), one can extend the coordinate of the lowest GL to infinity and set $d\psi/dz|_{z=\infty} = 0$ with $\psi|_\infty = 0$. Solving Eq. (14) with the latter boundary conditions, we arrive at

$$\psi = \frac{1}{(C + z/\sqrt{6}L_s)^2}, \tag{16}$$

where C satisfies the following equation:

$$C^3 - C/2 = (W_g/\sqrt{6}L_s). \tag{17}$$

Since in reality $W_g \gg \sqrt{6}L_s$, one obtains $C \simeq (W_g/\sqrt{6}L_s)^{1/3} \propto V_g^{1/6}$.

Taking into account Eq. (8), Eq. (16) yields

$$\mu_k \simeq \frac{eV_g}{2[C + (k-1)d/\sqrt{6}L_s]^2} = \mu_1 a_k. \tag{18}$$

Here

$$\mu_1 = \frac{eV_g}{2C^2} \propto \left(\frac{V_g}{W_g}\right)^{2/3} \tag{19}$$

is the Fermi energy of electrons in the topmost GL in the n section (holes in the p section)

$$a_k = [1 + (k-1)\gamma]^{-2} \tag{20}$$

and

$$\gamma = \frac{d}{\sqrt{6}L_s C} \propto \frac{d}{W_g^{1/3} L_s^{2/3}} \propto \left(\frac{V_g}{W_g}\right)^{1/3}. \tag{21}$$

Setting $d = 0.35$ nm, $W_g = 10$ nm, $\varkappa = 4$, and $V_g = 1$ V, one can obtain $L_s \simeq 0.44$ nm. $C \simeq 2.14$, $\mu_1 \simeq 109$ meV, and $\gamma \simeq 0.153$. The μ_k versus k dependence obtained using our simplified analytical model, i.e., given by Eqs. (15) and (17) is shown by a solid line in Fig. 5.

Equations (9)–(21) are valid when $\mu_K > k_B T$, i.e., at sufficiently large V_g or/and sufficiently small T. Since the Fermi energy (at fixed electron density) decreases with increasing temperature, the above formulas of our simplified (idealistic) model yield somewhat exaggerated values of this energy [compare the dependences in Fig. 5 obtained numerically using Eqs. (4)–(7) and that found analytically using Eqs. (18)–(21)].

V. REVERSE CURRENT

The current across the n-i-p junctions under their reverse bias [$V<0$, see Fig. 2(c)] is an important characteristic of such junctions.[21] In particular, this current can substantially affect the performance of the terahertz tunneling transit-time oscillators and interband photodetectors.[5,17] This current is associated with the thermogeneration and tunneling generation of the electron-hole pairs in the i region. A significant contribution to this current can be provided by the injection of minority carriers (holes in the n region and electrons in the p region). Such an injection current in the kth GL is determined by the height of the barrier for the minority carrier which, in turn, is determined by the Fermi energy μ_k of the majority carrier. The latter, as shown above, depends on the gate voltage and the GL index. As a result, the reverse current can be presented as

$$J = J_i + J_{th} + J_{tunn}, \tag{22}$$

where the injection current (which is assumed to be of the thermionic origin) is given by

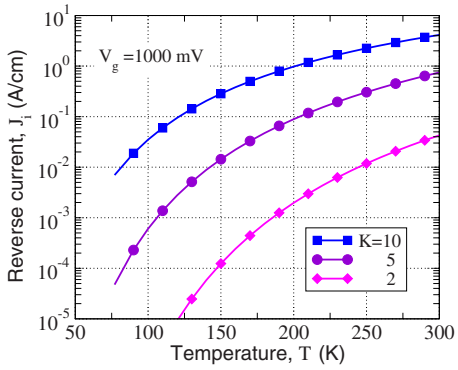

FIG. 6. (Color online) Temperature dependence of reverse current (injection component, J_i) for multiple-GL structures with different number of GLs.

$$J_i = \frac{2ev_F}{\pi^2}\left(\frac{k_BT}{\hbar v_F}\right)^2 \int_{-\pi/2}^{\pi/2} d\theta \cos\theta \times \sum_{k=1}^{K} \int_0^\infty \frac{d\xi\xi}{1+\exp(\xi+\mu_k/k_BT)}$$
$$= \frac{24ev_F\Sigma_T}{\pi^3}\sum_{k=1}^{K}\int_0^\infty \frac{d\xi\xi}{1+\exp(\xi+\mu_k/k_BT)},$$
$$= \frac{12J_T}{\pi^2}\sum_{k=1}^{K}\int_0^\infty \frac{d\xi\xi}{1+\exp(\xi+\mu_k/k_BT)} \tag{23}$$

with $J_T = 2ev_F\Sigma_T/\pi$. At $T=77-300$ K, $J_T \simeq 0.06-0.9$ A/cm. Deriving Eq. (24), we have taken into account that the distribution function of holes which enter the n region overcoming the barrier in the kth GL with the height μ_k is $f_k^{pn} \simeq \{1+\exp[(\mu_k+v_Fp)/k_BT]\}^{-1}$. Similar formula is valid for electrons in the p region. The factor 2 appears in Eq. (24) due to the contribution of both holes and electrons. Equation (24) is valid when the bias voltage is not too small: $eV > k_BT$. At $V \to 0$ one has $J_i \to 0$ (as well as J_{th} and J_{tunn}). Scattering of holes in the n region and electrons in the p region resulting in returning of portions of them back to the contacts leads to some decrease in J_i.

The temperature dependences of the reverse current associated with the injection from the n and p region calculated using Eq. (23) (with the quantities μ_k shown in Fig. 5) are presented in Fig. 6. As one might expect, the reverse current sharply increases with the temperature and the number of GL. The latter is due to relatively low-energy barriers for minority carriers in the n and p regions in GLs with large indices. For comparison, the injection current in a single-GL structure calculated using Eq. (23) with Eq. (8), is given by

$$J_i^S = \frac{12J_T}{\pi^2}\int_0^\infty \frac{d\xi\xi}{1+\exp(\xi+\mu_1/k_BT)}$$
$$\simeq \frac{12J_T}{\pi^2}\exp\left(-\frac{\hbar v_F\sqrt{æV_g/8eW_g}}{k_BT}\right). \tag{24}$$

At the same parameters as above and $T=300$ K, Eq. (24) yields $J_i^S \simeq 0.01$ A/cm.

When $K \gg \gamma^{-1}\sqrt{\mu_1/k_BT}$, the main contributions to the reverse current is associated with GLs with large indices (in which the barriers are very low) so that one obtains

$$J_i \lesssim KJ_T. \tag{25}$$

As follows from Eq. (25), the injection current (and, therefore, the net reverse current) can be fairly large due to the "shortcut" by GLs with large indices (placed deep below the gate).

Since the thermogeneration is associated primarily with the absorption of optical phonons,[21] the pertinent rate g_{th} is independent of the electric field in the i region, but it is proportional to the i-section length $2l$ ($l \lesssim L_g$). The contribution of the thermogeneration to the reverse current can be presented as

$$J_{th} = 4Kelg_{th}. \tag{26}$$

The quantity g_{th} as a function of the temperature was calculated in Ref. 20. Equations (23)–(26) are valid if $2l < l_R$, where l_R is the recombination length. In the situations when the bias voltage between the side contacts is not too small (as it should be, for instance, in GL-based interband photodetectors), the recombination length is fairly long. Indeed, assuming that the recombination time (at $T=300$ K) and the drift velocity are $\tau_R = 5\times10^{-10}$ s (Ref. 22) and $\langle v\rangle \sim v_F/2 = 5\times10^7$ cm/s,[23] respectively, one obtains $l_R \simeq 250$ μm.

Assuming that $2l=10$ μm with $g_{th}=10^{13}$ cm^{-2} s^{-1} and $g_{th}=10^{21}$ cm^{-2} s^{-1} at $T=77$ K and $T=300$ K, respectively,[22] we obtain $J_{th} \simeq 3.2\times(10^{-9}-10^{-1})$ A/cm. One can see that the thermogeneration contribution to the reverse current is much smaller than the injection contribution at lower temperatures while it can be substantial at $T=300$ K in the *n-i-p* structures with long i region.

The tunneling generation can significantly contribute to the reverse current at elevated electric fields in the i region, i.e., in relatively short GL structures at elevated bias voltages.[1,5] This current can be calculated using the following formula which follows from the expression for the tunneling probability in GLs (Refs. 1 and 2) (see, for instance, Ref. 5):

$$J_{tunn} = \frac{ev_F}{\pi^2 l^2}\left(\frac{eV}{2l\hbar v_F}\right)^{3/2} \propto \frac{V^{3/2}}{l^{1/2}}. \tag{27}$$

Depending on the *n-i-p* junction applications, the quantities V and l should be chosen to provide either domination of tunneling current (as in tunneling transit-time oscillators[4]) or its suppression (as in the interband photodetectors[17]).

VI. MULTIPLE-GL STRUCTURES WITH HIGHLY CONDUCTIVE BGL

As it was mentioned in the introduction, the multiple-GL structures obtained by the thermal decomposition from 4H-SiC substrate, include a highly conductive BGL. Its presence can strongly affect the potential and electron density distributions across the multiple-GL structure. However, the BGL influence depends on the connection between the BGL and the side contacts. The following options can be considered:

(a) *all the GLs are directly connected with the side contacts.* If the bias voltage between the side contacts $V=0$, the potentials of GLs with different indices $1 \leq k \leq K$ (the BGL index is equal to $K+1$) can be found using the same equations as above, i.e., Eqs. (4)–(7) or Eq. (14) but with modified boundary conditions. Considering high conductivity of BGL, its potential can be assumed to be constant and equal to the side contact potential, the second condition in Eq. (6) should be replaced by $\psi|_{z=z_{K+1}}=0$. In the case of multiple-GL structures with sufficiently large K, both $d\psi/dz$ and ψ steeply tend to zero with increasing z. This directly follows from Fig. 2 (see the curves calculated for $K=50$), as well as from Eqs. (16)–(21). Thus, the difference between the potential distributions calculated using the boundary conditions $d\psi/dz|_{z=z_K}=0$ and $\psi|_{z=z_{K+1}}=0$ is fairly small. Hence, the results obtained above are also applicable for the multiple-GL structures with the highly conductive BGL if $K \gg 1$. Since the highly conductive BGL effectively shorts out the side contacts, for the devices whose operation requires $V \neq 0$ the GBL should be cut between the side contacts. (b) *All the GLs, except the BGL, are connected with the side contacts and a bias voltage* V_b is applied between the GBL and one of the side contacts. In this case, the GBL can be considered as the back gate so that the potential distribution is determined by both V_g and V_b. However, in the absence of the top gates, the obtained results can still be used if W_g and V_g in all equations substituted with d and V_b, respectively. (c) *All the GLs, except the BGL, are connected with the side contacts, but the GBL is isolated from the side contacts.* In such a case, the GBL plays the role of a floating gate. This case needs a separate analysis and will be considered elsewhere.

VII. CONCLUSIONS

We calculated the Fermi energies and electron and hole densities in the electrically induced *n-i-p* junctions formed in multiple-GL structures as functions of the GL indices, gate voltage, temperature, and structural parameters. Using the obtained values of the Fermi energies and the heights of potential barriers for minority carriers in the *n* and *p* regions, we found the temperature dependences of the reverse injection current for multiple-GL structures with different numbers of GLs. This analysis shows the possibility of the formation of effective electrically induced *n* and *p* regions and *n-i-p* junctions, i.e., the *n-i-p* junctions with suppressed reverse currents in multiple-GL structures. These electrically induced *n-i-p* junctions in multiple-GL structures can be used in different devices, such as terahertz tunneling transit-time oscillators, lasers, and high-performance interband photodetectors. They could enhance the device performance (increasing output power and responsivity) and expand their functions by allowing for the gate-voltage control.

ACKNOWLEDGMENTS

This work was supported by the Japan Society for Promotion of Science and by the Japan Science and Technology Agency, CREST, Japan.

*m-ryzhii(at)u-aizu.ac.jp

[1] V. V. Cheianov and V. I. Fal'ko, Phys. Rev. B **74**, 041403(R) (2006).
[2] L. M. Zhang and M. M. Fogler, Phys. Rev. Lett. **100**, 116804 (2008).
[3] B. Huard, J. A. Sulpizio, N. Stander, K. Todd, B. Yang, and D. Goldhaber-Gordon, Phys. Rev. Lett. **98**, 236803 (2007).
[4] B. Özyilmaz, P. Jarillo-Herrero, D. Efetov, D. A. Abanin, L. S. Levitov, and P. Kim, Phys. Rev. Lett. **99**, 166804 (2007).
[5] V. Ryzhii, M. Ryzhii, V. Mitin, and M. S. Shur, Appl. Phys. Express **2**, 034503 (2009).
[6] M. Ryzhii and V. Ryzhii, Jpn. J. Appl. Phys., Part 2 **46**, L151 (2007).
[7] F. Xia, T. Murller, Y.-M. Lin, A. Valdes-Garsia, and F. Avouris, Nat. Nanotechnol. **4**, 839 (2009).
[8] V. Ryzhii and M. Ryzhii, Phys. Rev. B **79**, 245311 (2009).
[9] F. Varchon, R. Feng, J. Hass, X. Li, B. N. Nguyen, C. Naud, P. Mallet, J.-Y. Veuillen, C. Berger, E. H. Conrad, and L. Magaud, Phys. Rev. Lett. **99**, 126805 (2007).
[10] M. Orlita, C. Faugeras, P. Plochocka, P. Neugebauer, G. Martinez, D. K. Maude, A.-L. Barra, M. Sprinkle, C. Berger, W. A. de Heer, and M. Potemski, Phys. Rev. Lett. **101**, 267601 (2008).
[11] P. Neugebauer, M. Orlita, C. Faugeras, A.-L. Barra, and M. Potemski, Phys. Rev. Lett. **103**, 136403 (2009).
[12] M. Orlita and M. Potemski, Semicond. Sci. Technol. **25**, 063001 (2010).
[13] D. L. Miller, K. D. Kubista, G. M. Rutter, M. Ruan, W. A. de Heer, P. N. First, and J. A. Stroscio, Science **324**, 924 (2009).
[14] M. Sprinkle, D. Siegel, Y. Hu, J. Hicks, A. Tejeda, A. Taleb-Ibrahimi, P. Le Fèvre, F. Bertran, S. Vizzini, H. Enriquez, S. Chiang, P. Soukiassian, C. Berger, W. A. de Heer, A. Lanzara, and E. H. Conrad, Phys. Rev. Lett. **103**, 226803 (2009).
[15] V. Ryzhii, M. Ryzhii, A. Satou, T. Otsuji, A. A. Dubinov, and V. Ya. Aleshkin, J. Appl. Phys. **106**, 084507 (2009).
[16] V. Ryzhii, A. A. Dubinov, T. Otsuji, V. Mitin, and M. S. Shur, J. Appl. Phys. **107**, 054505 (2010).
[17] V. Ryzhii, M. Ryzhii, V. Mitin, and T. Otsuji, J. Appl. Phys. **107**, 054512 (2010).
[18] V. Ryzhii, M. Ryzhii, and T. Otsuji, Phys. Status Solidi A **205**, 1527 (2008).
[19] S. Luryi, Appl. Phys. Lett. **52**, 501 (1988); see also S. Luryi, in *High-Speed Semiconductor Devices*, edited by S. M. Sze (Wiley, New York, 1990), p. 57.
[20] H. Fukidome, Y. Miyamoto, H. Handa, E. Saito, and M. Suemitsu, Jpn. J. Appl. Phys. **49**, 01AH03 (2010).
[21] M. Shur, *Physics of Semiconductor Devices* (Prentice-Hall, New Jersey, 1990).
[22] F. Rana, P. A. George, J. H. Strait, J. Dawlaty, S. Shivaraman, M. Chandrashekhar, and M. G. Spencer, Phys. Rev. B **79**, 115447 (2009).
[23] R. S. Shishir, D. K. Ferry, and S. M. Goodnick, J. Phys.: Conf. Ser. **193**, 012118 (2009).